Postprint of: Nosko O., Vanhanen J., Olofsson U., Emission of 1.3–10 nm airborne particles from brake materials, AEROSOL SCIENCE AND TECHNOLOGY, Vol. 51, Iss. 1 (2017), pp. 91-96, DOI: 10.1080/02786826.2016.1255713

Title: Emission of 1.3–10 nm airborne particles from brake materials

Running title: 1.3–10 nm airborne particles from brake materials

Oleksii Nosko[*a], Joonas Vanhanen[b], Ulf Olofsson[a]

[a] Department of Machine Design, KTH Royal Institute of Technology,

Brinellvägen 83, Stockholm, 10044, Sweden

[b] Airmodus Ltd., Pietari Kalmin katu 1 F 1, Helsinki, 00560, Finland

Operation of transport vehicle brakes makes a significant contribution to airborne particulate matter in urban areas, which is subject of numerous studies due to the environmental concerns. We investigated the presence and number fractions of 1.3–10 nm airborne particles emitted from a low-metallic car brake material (LM), a non-asbestos organic car brake material (NAO) and a train brake cast iron against a cast iron. Particles were generated by a pin-on-disc machine in a sealed chamber and analysed using a nano Condensation Nucleus Counter, a CPC, and an FMPS. It was found that 1.3–4.4 nm particles are emitted during the friction. For the pairs with the LM and NAO, 1.3–4.4 nm particles predominate in number at temperatures above 160 °C. The emission of the 1.3–4.4 nm particles precedes the emission of above 4.4 nm particles. For the cast iron pair, the number of 1.3–4.4 nm particles is smaller than the number of 4.4–10 nm particles. The findings suggest that brake materials produce a significant number of 1.3–4.4 nm airborne particles, and these particles should not be neglected in environmental and tribological studies.

Key words: nanoparticles, airborne particles, brake wear, particle nucleation, critical temperature

[*] Corresponding author. E-mail: nosko@kth.se (O. Nosko).

1. Introduction

Emission of airborne particulate matter has been one of the interesting and essential research subjects due to the environmental and health concerns. Strong correlations were found between various adverse health effects and high concentrations of particles in the atmosphere (Pope III et al., 2002; Oberdörster et al., 2005). In urban environments, and especially in the vicinity of traffic arteries, a significant fraction of airborne particulate matter originates from transport vehicles (Pant and Harrison, 2013; Vu et al., 2015). Recent studies revealed that one of the main transport-related sources of particles is the operation of brakes (Thorpe and Harrison, 2008; Gietl et al., 2010).

There are two mechanisms of aerosol particle generation in brakes. During braking the sliding surfaces are worn out and some of the *wear particles* become airborne and are released to the atmosphere. Simultaneously, the sliding surfaces are frictionally heated, which is accompanied by the generation of vapours. The interaction of the vapours with the air results in the *nucleation of nanoparticles* and their subsequent clustering (Namgung et al., 2016). Depending on the diameter, particles have different chances to penetrate the human body through inhalation, ingestion, or skin contact and then reach the internal organs (Oberdörster, 2001; Gasser et al., 2009).

Many studies have been devoted to counting and size classification of airborne particles from sliding contacts. Garg et al. (2000) performed a brake dynamometer study of emissions of particles larger than 10 nm in aerodynamic diameter from car brakes with non-asbestos organic pads (NAO) and semi-metallic pads (SM). Sanders et al. (2003) made measurements of size distributions of above 30 nm aerodynamic diameter particles from car brakes with low-metallic (LM), NAO and SM pads, using a brake dynamometer and testing a vehicle in a wind tunnel and on a test track. Iijima et al. (2007) classified by size abrasion dusts with above 500 nm aerodynamic diameters, emitted from a car brake dynamometer with NAO pads. Olofsson et al. (2009) investigated emissions of above 10 nm particles from a steel pin-on-disc pair. Wahlström et al. (2010, 2012) conducted studies of above 10 nm particles from LM and NAO car brake materials against cast iron, using a pin-on-disc machine and a disc brake assembly test stand. Kukutschová et al. (2011) performed a study of above 10 nm particles from a car brake dynamometer with LM pads. Olofsson (2011) investigated above 10 nm particles on a pin-on-disc machine with the pin and disc samples cut from the steel train brake block and wheel, respectively. Abbasi et al. (2011, 2012) carried out studies of above 10 nm particles from organic and sintered train brake materials against steel, using a pin-on-disc machine and conducting field tests. Alemani et al. (2015) and Nosko et al. (2015) performed pin-on-disc studies of above 5.6 nm particles emitted from LM and NAO car brake materials against cast iron. Namgung et al. (2016) investigated above 5.6 nm particles emitted from a metro train brake dynamometer with NAO pads. An extensive review of the relevant literature can be found in Grigoratos and Martini (2015) and Kumar et al. (2013).

It appears from the abovementioned studies that airborne brake particles have been comprehensively investigated for the diameter range above 5.6 nm. The question of the presence of smaller brake particles and their number fraction remains still unexplored due to measurement limitations. The instruments relying on electrical detection of particles are inapplicable for counting below 5 nm particles since such small particles have a low charging probability. The conventional commercial condensation particle counters do not allow detecting particles smaller than 2.5 nm. The purpose of the present study was to experimentally quantify the number fraction of 1.3–4.4 nm airborne particles emitted from the brake friction pairs of LM / cast iron, NAO / cast iron, and cast iron / cast iron using a novel measurement technique.

2. Experimental

Airborne particles were generated by using the pin-on-disc machine depicted in Fig.1. This set-up was proposed by Olofsson et al. (2009). The pin sample was a cylinder with a diameter of 10 mm. A dead weight pressed it against a horizontally positioned disc sample with a pressure of 1 MPa. The average friction radius was 25 mm. The disc sample, with an outer diameter of 63 mm and a thickness of 6 mm, was driven by a motor. The temperature T in the disc sample was measured by a chromel–alumel thermocouple. The junction of the thermocouple, 0.5 mm in diameter, was installed at the average friction radius at a distance of 3 mm from the friction surface.

Figure 1

The pin samples were milled from a LM car brake pad, a NAO car brake pad, and a cast iron train brake block. The disc samples were milled from a car brake disc made of a perlitic lamellar cast iron. The original friction surfaces remained unaltered during the milling. Table 1 presents the elemental compositions of the sample materials (Alemani et al., 2015; Matějka et al., 2016). Each of the three pin sample materials was tested three times.

Table 1

The duration of the tests was 90 min. In each test, the sliding velocity at the average friction radius increased linearly from zero to a value v_s during 60 min, and then it decreased linearly to zero during 30 min. The value v_s was set depending on the friction pair. Car brakes normally work at temperatures below 200 °C (Garg et al., 2000). Therefore, for the LM and NAO v_s was set equal to 1.2 m/s and 1.7 m/s, respectively, which provided an increase in T to about 180 °C. In the test with the cast iron pair, v_s = 0.5 m/s.

The pin-on-disc machine was located in a sealed chamber. A fan drew the room air in the chamber via a HEPA filter and an inlet with a rate of 130 L/min. The filter removed particles from the passing air. The air flow inside the chamber picked up particles generated at the sliding contact between the pin sample and disc sample and carried them to the air outlet. The sealed chamber thus excluded external sources of particles.

The air coming out of the chamber was analysed by three aerosol measurement instruments: an Airmodus A11 nano Condensation Nucleus Counter (nCNC), a TSI Condensation Particle Counter 3772 (CPC), and a TSI Fast Mobility Particle Sizer 3091 (FMPS). Table 2 presents the characteristics of the instruments.

Table 2

The CPC counts particles larger than 10 nm. The FMPS separates 5.6–560 nm particles into 32 stages using an electrostatic classification technique. The nCNC is an instrument based on two stages of condensational particle growth followed by optical counting (Vanhanen et al., 2011). At the first stage, a Particle Size Magnifier grows aerosol nanoparticles up to about 90 nm in mobility diameter with diethylene glycol condensation. At the second stage, a laminar flow condensation particle counter grows the particles up to optically detectable diameters using n-butanol as a working fluid and counts them. The nCNC allows measuring the number concentration of particles with diameters from 1.3 nm

to 1000 nm. The calibration of the nCNC was done using NiCr oxide particles produced with a hot wire generator and size selected by a high resolution Differential Mobility Analyser (Kangasluoma et al., 2013). The nCNC operated in a so-called stepping mode. The lower cut size of the instrument changed step-wise between 1.3 nm and 4.4 nm every 30 s. For each cut size, an average particle concentration was recorded. Thus, the nCNC indicated the concentration of above 1.3 nm particles, denoted as 'nCNC1.3', and the concentration of above 4.4 nm particles, denoted as 'nCNC4.4', with 60 s sampling interval.

To minimise losses of particles during the measurement, the sampling tubes connecting the chamber air outlet and the instrument aerosol inlets had minimum possible lengths. The nCNC sampling tube was straight. The particle penetration ratio through the sampling tube was calculated, depending on the sampling tube length, aerosol flow rate, and particle diameter (see Table 2). The calculations were made according to Gormley and Kennedy (1949).

3. Results

Figure 2 presents the test results for the LM. During the first 25 min, the concentrations measured by the nCNC and CPC are low. In the interval from 25 to 53 min, they rise to a level of 10^2 no/cm^3. At about 53 min, when $T \approx 160$ °C, the particle emission intensifies, with the concentrations increasing to above 10^5 no/cm^3. The nCNC4.4 and CPC measurements agree well with those made by the FMPS. The concentrations are not shown in the intervals in which they exceed the corresponding maximum measurable limits (see Table 2). It is important to note that the nCNC1.3 concentration starts to increase about 3 min earlier than the nCNC4.4 and CPC concentrations. The maximum value of T is 180 °C. As T goes below 160 °C, the concentrations decay.

Figure 2

The test results obtained for the NAO are shown in Fig.3. They are qualitatively similar to the results presented in Fig.2, although the concentrations do not exceed the maximum measurable limits. In this test, T is slightly lower, with a maximum value of 178 °C. The particle emission intensification is observed at $T \approx 160$ °C. The concentrations and T reach their maximum values almost at the same time instance.

Figure 3

Figure 4 shows the results for the cast iron pair. As T rises to 74 °C, the concentrations measured by the nCNC and CPC increase to above 10^3 no/cm^3. It is noteworthy that the nCNC1.3 concentration is higher than 10 no/cm^3 during the whole test, while the nCNC4.4 and CPC concentrations are below this level at the beginning and the end of the test.

Figure 4

Figure 5 presents number fractions of particles for different diameter ranges, based on the measurement data from the nCNC and CPC. The fractions of 1.3–4.4 nm particles and 4.4–10 nm particles were determined as the difference in the nCNC1.3 and nCNC4.4 concentrations and the difference in the nCNC4.4 and CPC concentrations, respectively. It is shown that the friction pairs produce a significant number of 1.3–4.4 nm particles. The particle number percentage for the LM and

NAO is dependent on T. For example, at $T \approx 150$ °C the number of above 10 nm particles is larger than the number of 1.3–4.4 nm particles, while the fraction of 4.4–10 nm particles is almost zero. By contrast, at $T \approx 175$ °C the 1.3–4.4 nm particles are predominant, and there is a noticeable fraction of 4.4–10 nm particles. For the cast iron pair, the number of 1.3–4.4 nm particles is smaller than the number of 4.4–10 nm particles, while the total number of 1.3–10 nm particles is approximately equal to the number of above 10 nm particles.

Figure 5

Figure 6 shows size distributions of 5.6–100 nm particles measured by the FMPS and normalised in the interval 5.6 to 560 nm. For the LM and NAO, we have zero distributions at $T \approx$ 150 °C, i.e. the particles detected by the FMPS are larger than 100 nm. However, at $T \approx 175$ °C almost 100 % of the particles are in the diameter range 5.6 to 40 nm, with a modal diameter of 11 nm. Considering the cast iron pair, most of the particles generated by this pair have diameters above 100 nm. The FMPS also indicates the presence of 5.6–10 nm particles.

Figure 6

Repetitions of the tests under the same conditions confirmed reproducibility of the obtained results. A significant difference was only observed in the maximum particle concentration attained during the test for the pairs with the LM and NAO. This difference was most probably caused by uncontrolled fluctuations in T (of the order of 1 ºC).

4. Discussion

The measurement data from the nCNC and CPC shown in Fig.5 reveal the presence of 1.3–4.4 nm particles, as well as 4.4–10 nm particles in the specific cases. These data agree qualitatively with the FMPS distributions of Fig.6. For the pairs with the LM and NAO, both nCNC and FMPS indicate no particles in the diameter ranges of 4.4–10 nm and 5.6–10 nm, respectively, at $T \approx 150$ °C. On the other hand, both nCNC and FMPS detect particles in the mentioned ranges for the LM and NAO at $T \approx$ 175 °C and for the cast iron pair.

According to Figs.2 and 3, the particle emission from the pairs with the LM and NAO intensifies drastically at the critical temperature $T \approx 160$ °C. Similar temperature-related phenomena were previously observed. For example, Garg et al. (2000) found that the emission rate of 10–30 nm particles from brakes with NAO and SM pads increases by 1 to 2 orders of magnitude as the rotor temperature rises from 200 to 400 °C. Kukutschová et al. (2011) observed a substantial increase in the concentration of above 10 nm particles emitted from a brake with LM pads as the rotor temperature approached 300 °C. Wahlström at al. (2012) observed a 2 to 3 orders of magnitude increase in the concentration of above 20 nm particles from a LM pin sample against cast iron as the pin sample temperature rose from 170 to 240 °C. Alemani et al. (2015) tested LM and NAO materials against cast iron on the pin-on-disc machine used in the present study. FMPS measurements showed a predominance of 11–34 nm particles as the disc temperature exceeded a critical level of 165–190 °C, which matches the corresponding particle size distributions of Fig.6. The mentioned critical temperature (165–190 °C) was determined by analysing the FMPS concentration of particles larger than 5.6 nm. The critical temperature obtained in this study ($T \approx 160$ °C) was determined in a similar way although based on the nCNC1.3 concentration of above 1.3 nm particles.

Analysis of the experimental data shows that the concentration of 1.3–4.4 nm particles noticeably increases even at relatively low temperatures. This is clearly seen for the pairs with the LM and NAO at $T \approx 120$ °C (see Figs.2 and 3) and for the cast iron pair at $T \approx 50$ °C (see Fig.4). The results for the LM and NAO can be explained by the generation of nanoparticles through the nucleation mechanism, which is in line with the study by Namgung et al. (2016) who observed an intensification of 5.6–40 nm particle emissions from a brake with NAO pads at disc temperatures above 70 °C. Note that the intensive emission of 1.3–4.4 nm particles at $T \approx 160$ °C preceded the emission of above 4.4 nm particles. Consequently, the formation of the above 4.4 nm particles could occur through clustering of the 1.3–4.4 nm particles (Kulmala et al., 2013). As for the cast iron pair, one can speculate that the temperature of the pin and disc samples was too low to generate vapours. Instead we could have a mechanical removal of metal oxides from the sliding surfaces, which produced solid nanoparticles of the metal oxides. Further research is necessary to enhance the understanding of the particle formation processes.

5. Conclusions

The main quantitative findings of the present study can be summarised as follows:

1. The three friction pairs considered produce a significant number of 1.3–4.4 nm airborne particles.
2. For the pairs with the LM and NAO, the number of 1.3–4.4 nm particles is predominant at temperatures above 160 °C. The emission of the 1.3–4.4 nm particles precedes the emission of above 4.4 nm particles.
3. For the cast iron pair, the number of 1.3–4.4 nm particles is smaller than the number of 4.4–10 nm particles.

Acknowledgement

The research received funding from the European Union Seventh Framework Programme (FP-PEOPLE-2012-IAPP) under the Rebrake Project, grant agreement no. 324385.

References

[1] Abbasi, S., Wahlström, J., Olander, L., Larsson, C., Olofsson, U., Sellgren, U. (2011). A study of airborne wear particles generated from organic railway brake pads and brake discs. Wear 273: 93–99.

[2] Abbasi, S., Jansson, A., Olander, L., Olofsson, U., Sellgren, U. (2012). A pin-on-disc study of the rate of airborne wear particle emissions from railway braking materials. Wear 284–285: 18–29.

[3] Alemani, M., Nosko, O., Metinoz, I., Olofsson, U. (2015). A study on emission of airborne wear particles from car brake friction pairs. SAE Int. J. Mater. Manuf. 9: 147–157.

[4] Garg, B.D., Cadle, S.H., Mulawa, P.A., Groblicki, P.J. (2000). Brake wear particulate matter emissions. Environ. Sci. Technol. 34: 4463–4469.

[5] Gasser, M., Riediker, M., Mueller, L., Perrenoud, A., Blank, F., Gehr, P., Rothen-Rutishauser, B. (2009). Toxic effects of brake wear particles on epithelial lung cells in vitro. Part. Fibre Toxicol. 6, No. 30.

[6] Gietl, J.K., Lawrence, R., Thorpe, A.J., Harrison, R.M. (2010). Identification of brake wear particles and derivation of a quantitative tracer for brake dust at a major road. Atmos. Environ. 44: 141–146.

[7] Gormley, P.G., Kennedy, M. (1949). Diffusion from a stream flowing through a cylindrical tube. Proc. R. Irish Acad. 52 (A): 163–169.

[8] Grigoratos, T., Martini, G. (2015). Brake wear particle emissions: A review. Environ. Sci. Pollut. Res. 22: 2491–2504.
[9] Iijima, A., Sato, K., Yano, K., Tago, H., Kato, M., Kimura, H., Furuta, N. (2007). Particle size and composition distribution analysis of automotive brake abrasion dusts for the evaluation of antimony sources of airborne particulate matter. Atmos. Environ. 41: 4908–4919.
[10] Kangasluoma, J., Junninen, H., Lehtipalo, K., Mikkilä, J., Vanhanen, J., Attoui, M., Sipilä, M., Worsnop, D., Kulmala, M., Petäjä, T. (2013). Remarks on ion generation for CPC detection efficiency studies in sub-3-nm size range. Aerosol Sci. Technol. 47: 556–563.
[11] Kukutschová, J., Moravec, P., Tomášek, V., Matějka, V., Smolík, J., Schwarz, J., Seidlerová, J., Šafářová, K., Filip, P. (2011). On airborne nano/micro-sized wear particles released from low-metallic automotive brakes. Environ. Pollut. 159: 998–1006.
[12] Kulmala, M., Kontkanen, J., Junninen, H., Lehtipalo, K., Manninen, H.E., Nieminen, T., Petäjä, T., Sipilä, M., Schobesberger, S., Rantala, P., Franchin, A., Jokinen, T., Järvinen, E., Äijälä, M., Kangasluoma, J., Hakala, J., Aalto, P.P., Paasonen, P., Mikkilä, J., Vanhanen, J., Aalto, J., Hakola, H., Makkonen, U., Ruuskanen, T., Mauldin III, R.L., Duplissy, J., Vehkamäki, H., Bäck, J., Kortelainen, A., Riipinen, I., Kurtén, T., Johnston, M.V., Smith, J.N., Ehn, M., Mentel, T.F., Lehtinen, K.E.J., Laaksonen, A., Kerminen, V.-M., Worsnop, D.R. (2013). Direct observations of atmospheric aerosol nucleation. Science 339: 943–946.
[13] Kumar, P., Pirjola, L., Ketzel, M., Harrison, R.M. (2013). Nanoparticle emissions from 11 non-vehicle exhaust sources — A review. Atmos. Environ. 67: 252–277.
[14] Matějka, V., Metinöz, I., Alemani, M., Wahlström, J., Bonfanti, A., Oloffson, U., Perricone, G. (2016). Dependency of PM10 particles emission on stability of friction coefficient and character of friction surface. Proceedings of Europe's Braking Conference and Exhibition 2016, Milan, EB2016-MDS-009.
[15] Namgung, H.-G., Kim, J.-B., Woo, S.-H., Park, S., Kim, M., Kim, M.-S., Bae, G.-N., Park, D., Kwon, S.-B. (2016). Generation of nanoparticles from friction between railway brake disks and pads. Environ. Sci. Technol. 50: 3453−3461.
[16] Nosko, O., Alemani, M., Olofsson, U. (2015). Temperature effect on emission of airborne wear particles from car brakes. Proceedings of Europe's Braking Conference and Exhibition 2015, Dresden, EB2015-TEF-014.
[17] Oberdörster, G. (2001). Pulmonary effects of inhaled ultrafine particles. Int. Arch. Occup. Environ. Health 74: 1–8.
[18] Oberdörster, G., Maynard, A., Donaldson, K., Castranova, V., Fitzpatrick, J., Ausman, K., Carter, J., Karn, B., Kreyling, W., Lai, D., Olin, S., Monteiro-Riviere, N., Warheit, D., Yang, H., A report from the ILSI Research Foundation/Risk Science Institute Nanomaterial Toxicity Screening Working Group. (2005). Principles for characterizing the potential human health effects from exposure to nanomaterials: Elements of a screening strategy. Part. Fibre Toxicol. 2, No. 8.
[19] Olofsson, U., Olander, L., Jansson, A. (2009). A study of airborne wear particles generated from a sliding contact. J. Tribol. 131, 044503.
[20] Olofsson, U. (2011). A study of airborne wear particles generated from the train traffic — Block braking simulation in a pin-on-disc machine. Wear 271: 86–91.
[21] Pant, P., Harrison, R.M. (2013). Estimation of the contribution of road traffic emissions to particulate matter concentrations from field measurements: A review. Atmos. Environ. 77: 78–97.
[22] Pope III, C.A., Burnett, R.T., Thun, M.J., Calle, E.E., Krewski, D., Ito, K., Thurston, G.D. (2002). Lung cancer, cardiopulmonary mortality, and long-term exposure to fine particulate air pollution. J. Am. Med. Ass. 287: 1132–1141.

[23] Sanders, P.G., Xu, N., Dalka, T.M., Maricq, M.M. (2003). Airborne brake wear debris: Size distributions, composition, and a comparison of dynamometer and vehicle tests. Environ. Sci. Technol. 37: 4060–4069.
[24] Thorpe, A., Harrison, R.M. (2008). Sources and properties of non-exhaust particulate matter from road traffic: A review. Sci. Total Environ. 400: 270–282.
[25] Vanhanen, J., Mikkilä, J., Lehtipalo, K., Sipilä, M., Manninen, H.E., Siivola, E., Petäjä, T., Kulmala, M. (2011). Particle size magnifier for nano-CN detection. Aerosol Sci. Technol. 45: 533–542.
[26] Vu, T.V., Delgado-Saborit, J.M., Harrison, R.M. (2015). Review: Particle number size distributions from seven major sources and implications for source apportionment studies. Atmos. Environ. 122: 114–132.
[27] Wahlström, J., Söderberg, A., Olander, L., Jansson, A., Olofsson, U. (2010). A pin-on-disc simulation of airborne wear particles from disc brakes. Wear 268: 763–769.
[28] Wahlström, J., Olander, L., Olofsson, U. (2012). A pin-on-disc study focusing on how different load levels affect the concentration and size distribution of airborne wear particles from the disc brake materials. Tribol. Lett. 46: 195–204.

Figure captions (All figures — colour online only)

Fig.1. Schematic of the experimental set-up

Fig.2. Particle concentrations and temperature T for the LM

Fig.3. Particle concentrations and temperature T for the NAO

Fig.4. Particle concentrations and temperature T for the cast iron pair

Fig.5. Particle number fractions

Fig.6. Normalised size distributions of 5.6–100 nm particles

Table 1. Elemental compositions of the sample materials, wt. %

Element	LM pin sample	NAO pin sample	Cast iron pin sample	Cast iron disc sample
Mg	10.4	2.6		
Al	9.1	1.1		
Si	5.8	3.9	1.64	1.7
Mn			0.59	0.57
P	0.9	0.01	1.08	0.03
S	5.2	6.4	0.22	0.26
K	0.67	4.0		
Ca	5.0	2.3		
Ti	0.17	9.0	0.07	
Cr	3.3	0.05	0.14	0.2
Fe	7.1	0.88	92.8	93.6
Cu	5.4	2.7		0.24
Zn	12.5	0.05		
Sr	0.01	0.46		
Zr	0.14	15.3		
Mo		0.89		
Sn	8.8	1.7		
Ba		27.7		
Bi	0.81			
C	22.4	19.8	3.5	3.4
F	2.1	0.47		

Table 2. Characteristics of the aerosol measurement instruments

Instrument	nCNC		CPC	FMPS
Operation mode	nCNC1.3	nCNC4.4		
Minimum measurable particle diameter, nm	1.3	4.4	10	5.6
Maximum measurable particle diameter, nm	1000		3000	560
Minimum measurable concentration, no/cm^3	~1	~1	~10^{-1}	$10^{2\,a}$
Maximum measurable concentration, no/cm^3	10^5		10^4	$10^{7\,a}$
Sampling interval, s	60		1	1
Aerosol inlet flow rate, L/min	2.5		1	10
Sampling tube length, cm	20		40	100
Particle penetration ratio through the sampling tube, %	73 [a]	92 [a]	94 [a]	95 [a]

[a] The value corresponds to the minimum measurable particle diameter

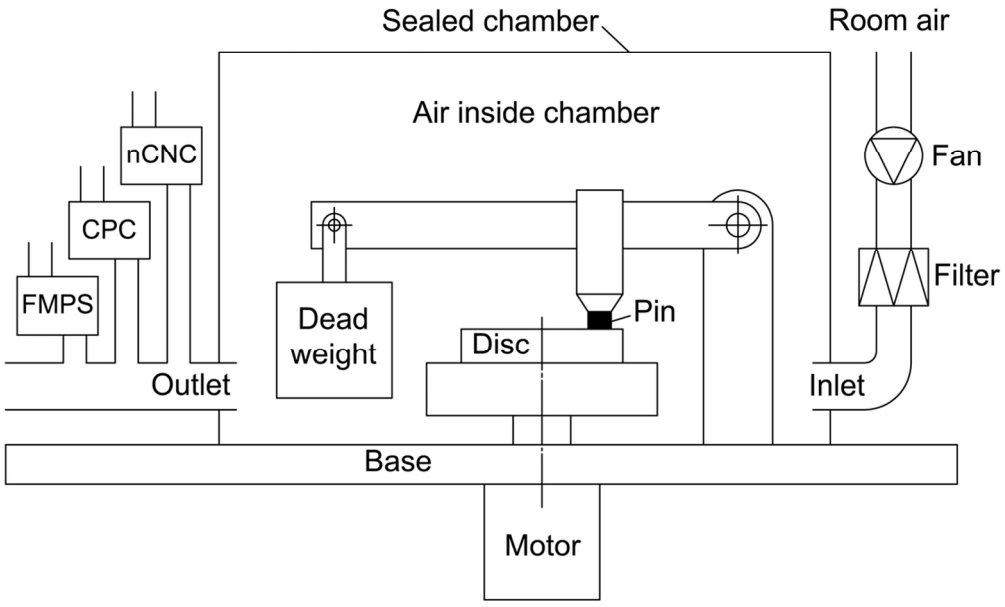

Figure 1

55x38mm (600 x 600 DPI)

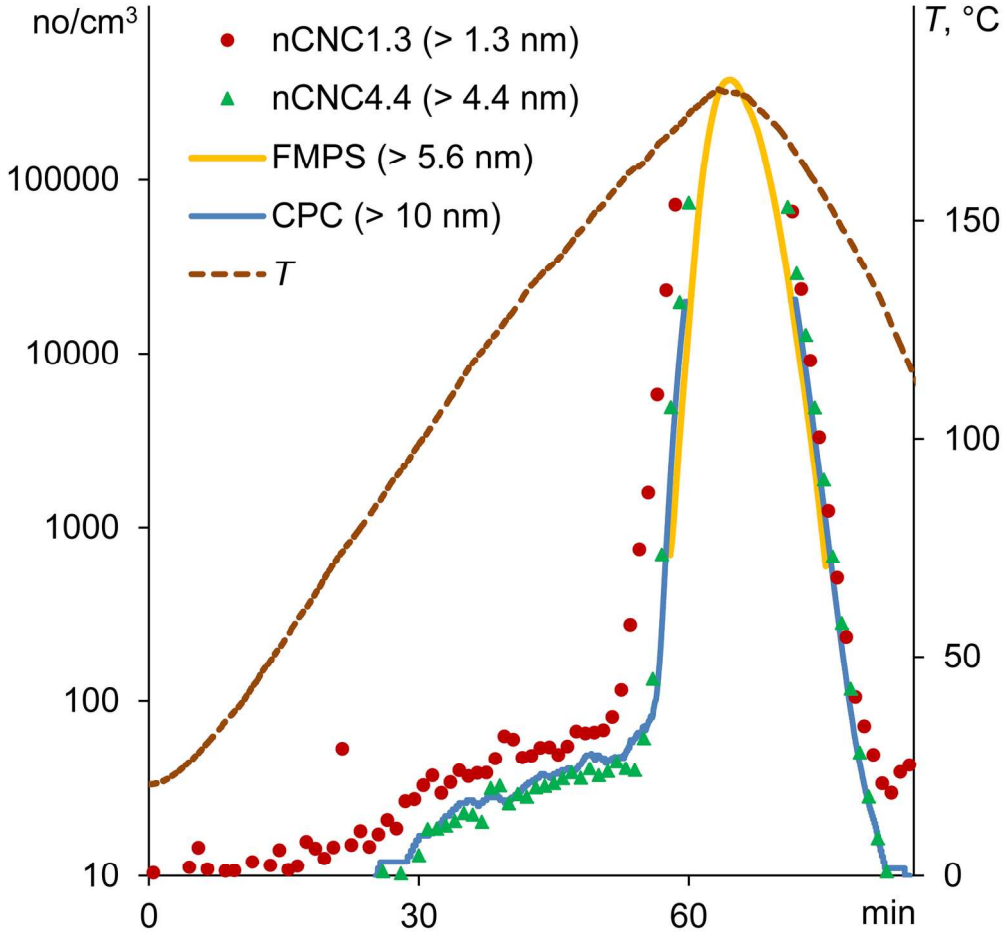

Figure 2

80x80mm (600 x 600 DPI)

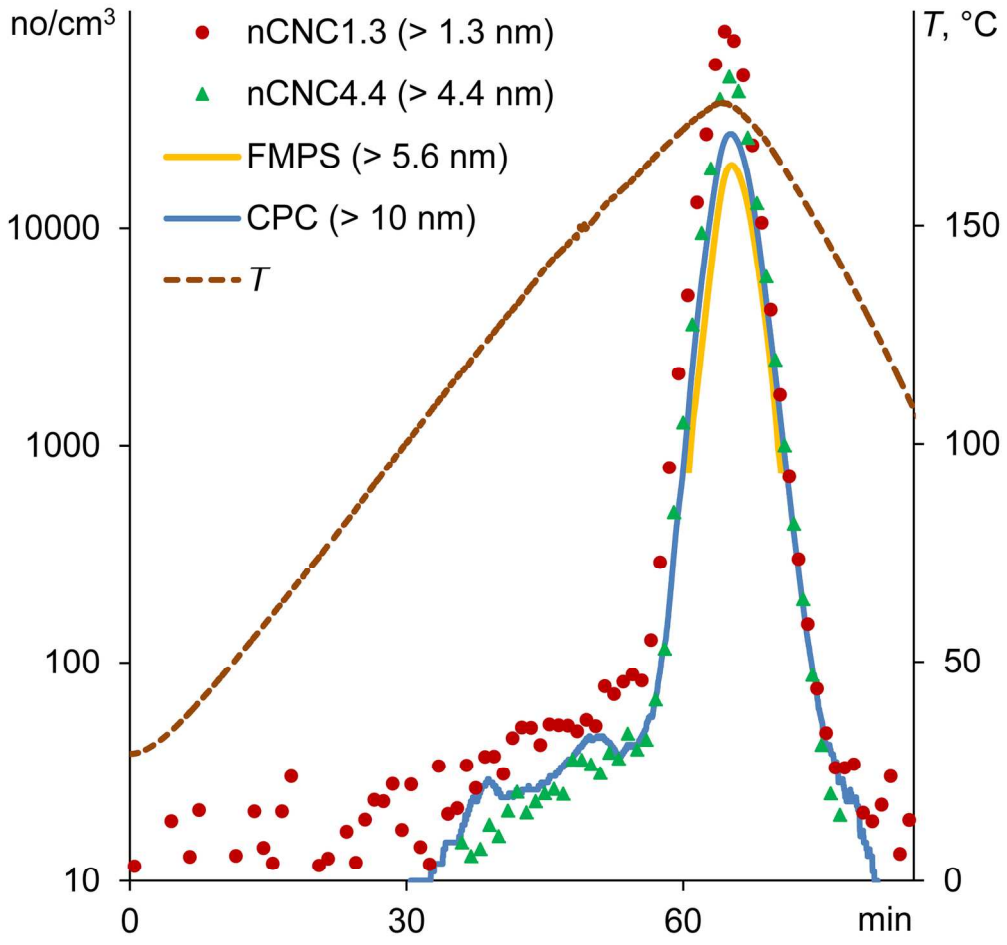

Figure 3

80x80mm (600 x 600 DPI)

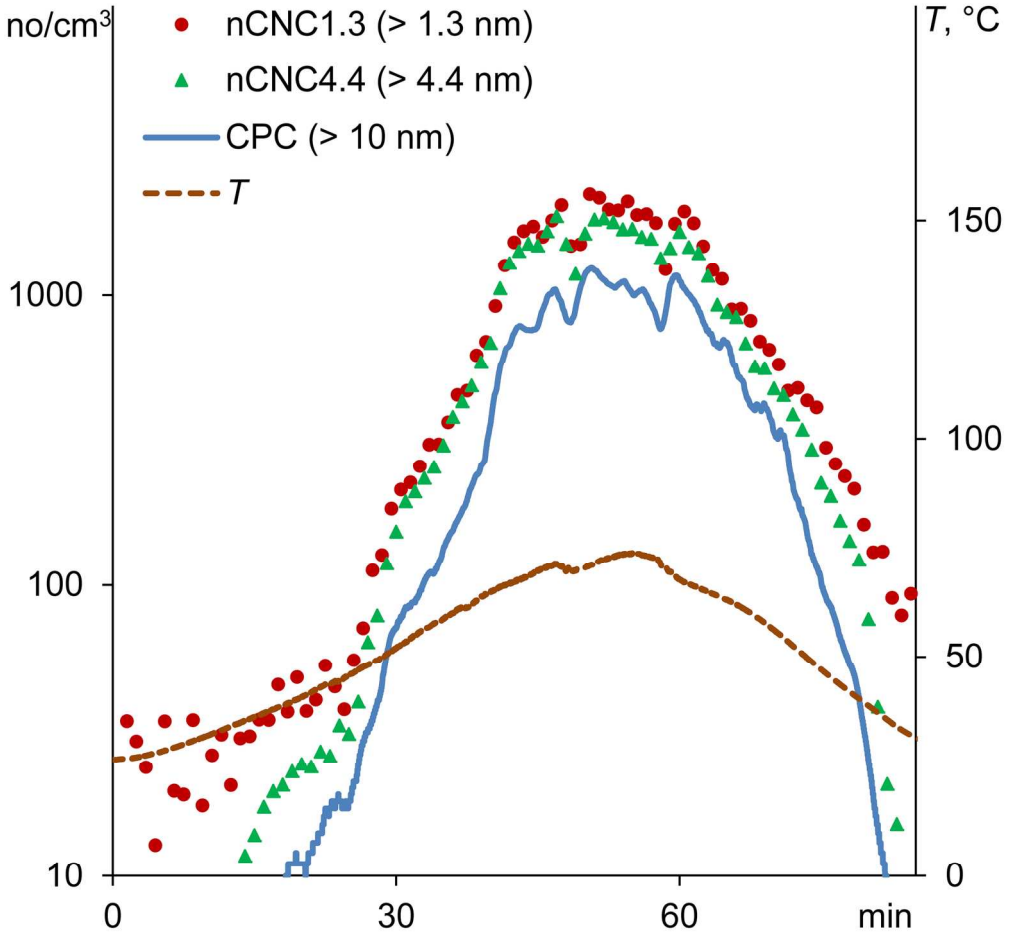

Figure 4

80x80mm (600 x 600 DPI)

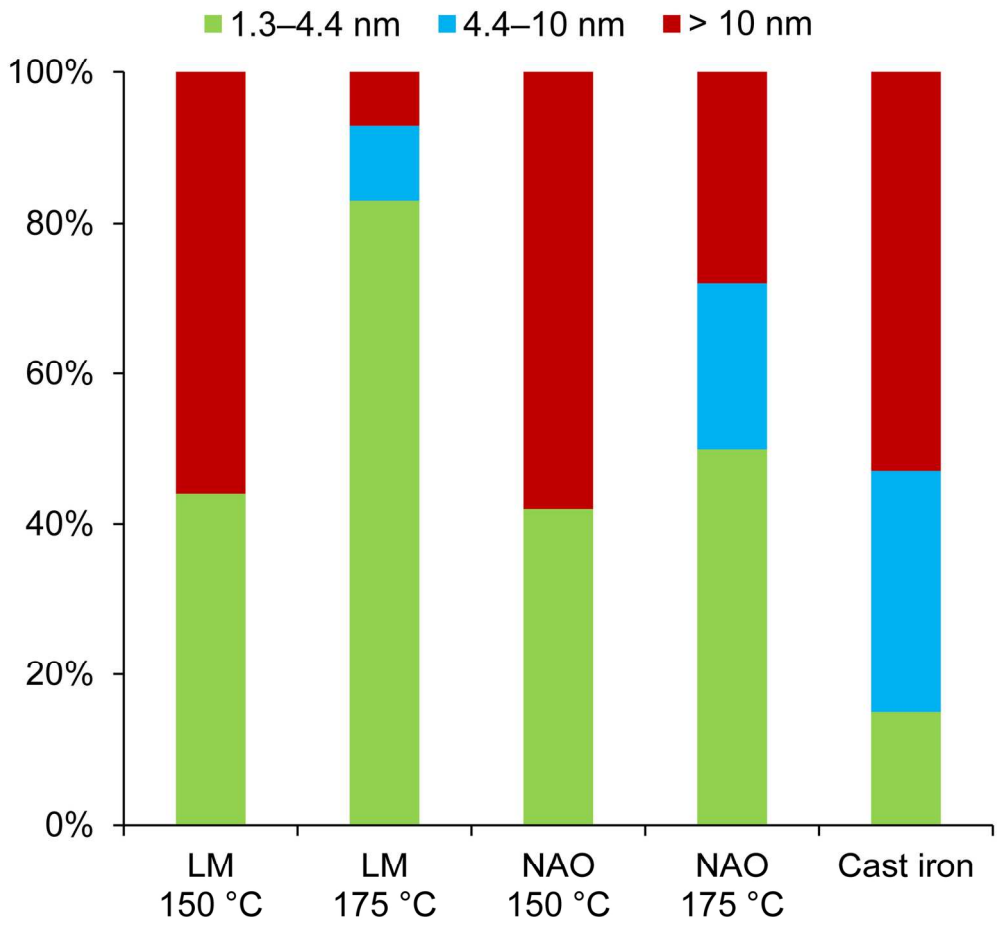

Figure 5

80x80mm (600 x 600 DPI)

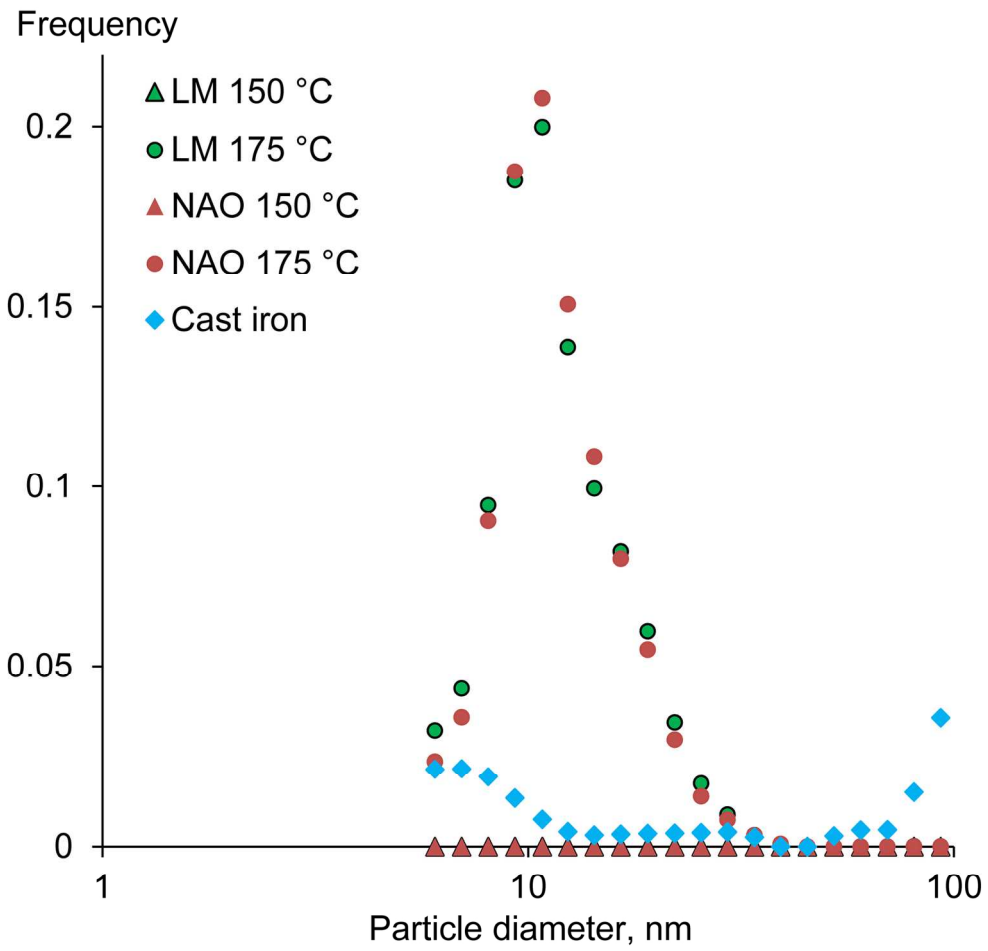

Figure 6

80x80mm (600 x 600 DPI)

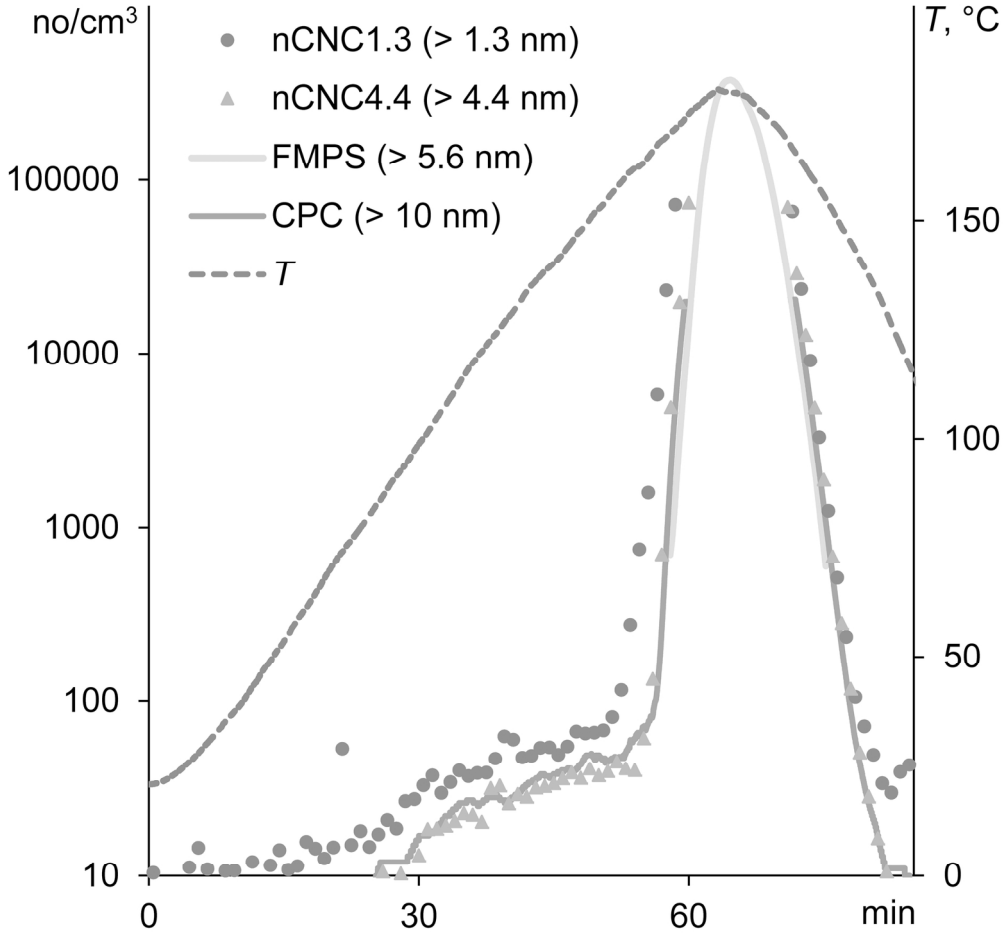

Figure 2 grey for the print version

80x80mm (600 x 600 DPI)

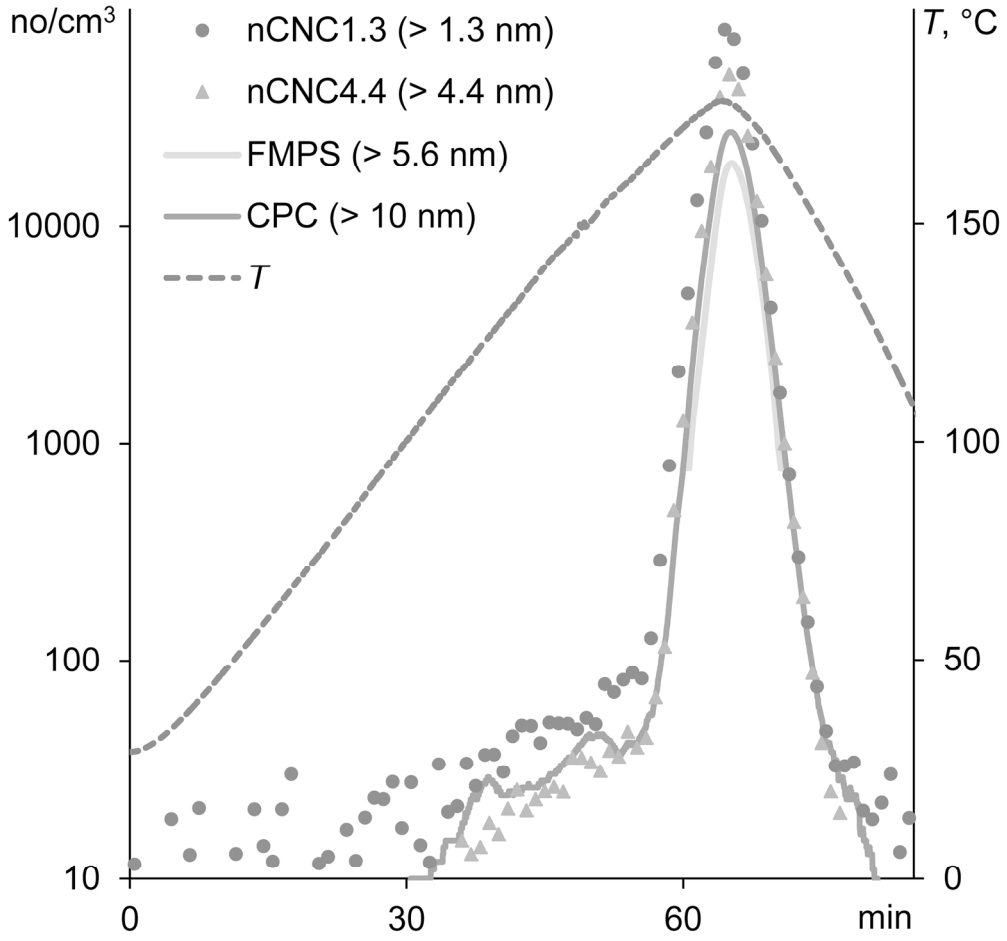

Figure 3 grey for the print version

80x80mm (600 x 600 DPI)

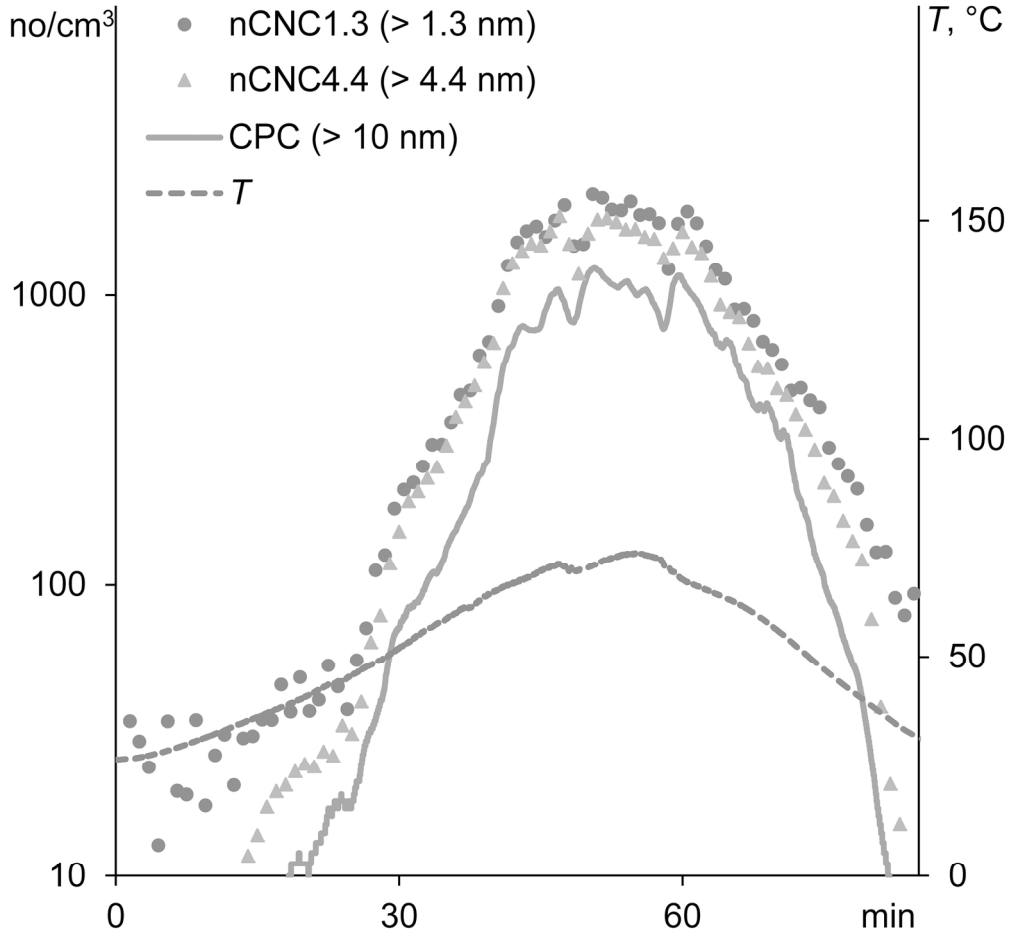

Figure 4 grey for the print version

80x80mm (600 x 600 DPI)

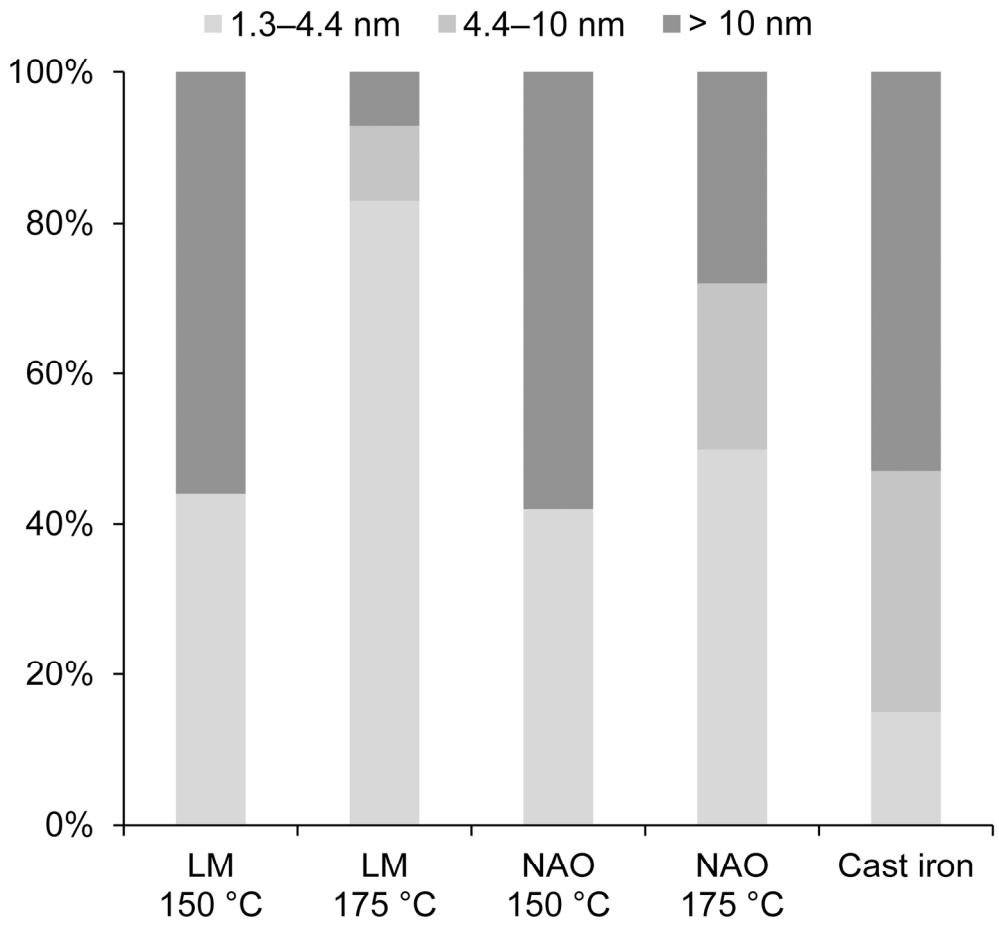

Figure 5 grey for the print version

80x80mm (600 x 600 DPI)

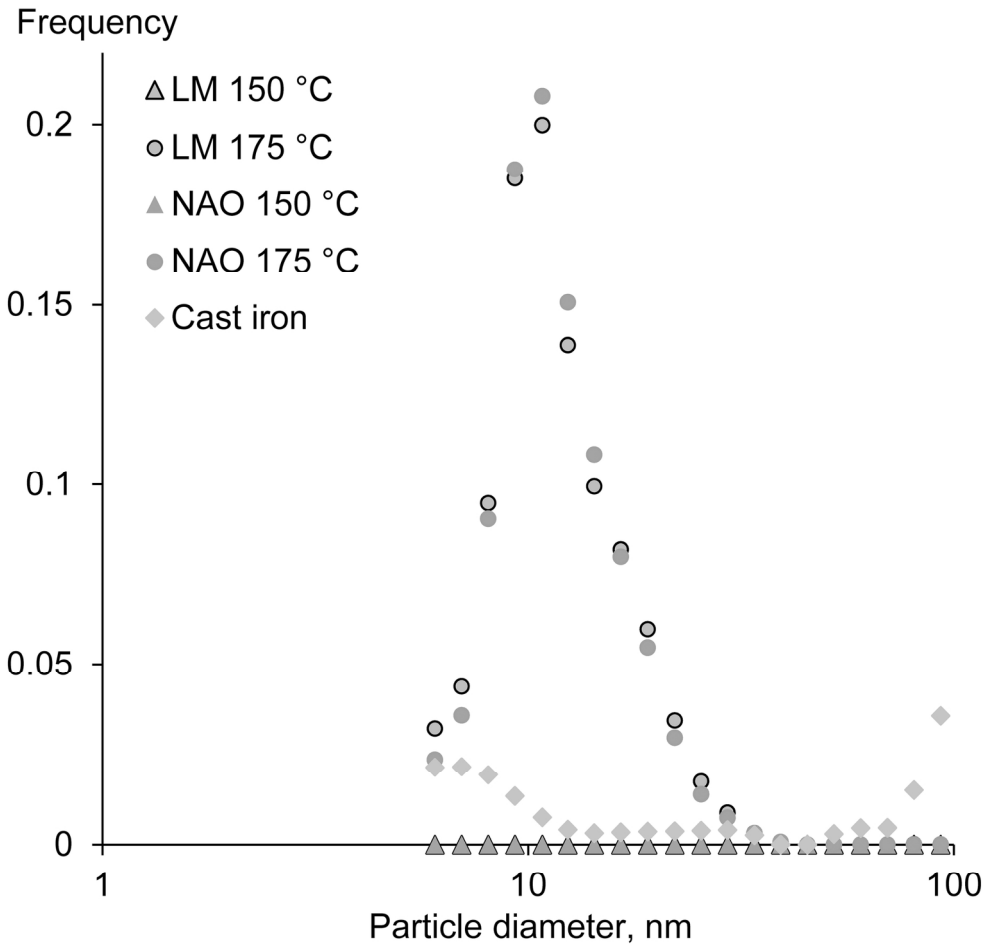

Figure 6 grey for the print version

80x80mm (600 x 600 DPI)